Heterogeneous nucleation of solid Al from the melt by TiB2 and Al3Ti: An ab initio molecular dynamics study

Heterogeneous nucleation of solid Al from the melt by TiB_2 and Al_3Ti: An *ab initio* molecular dynamics study

Junsheng Wang,[1] Andrew Horsfield,[1] Udo Schwingenschlögl,[2] and Peter D. Lee[1]
[1]*Department of Materials, Imperial College, London SW7 2AZ, United Kingdom*
[2]*PSE Division, King Abdullah University of Science and Technology, Thuwal 23955-6900, Saudi Arabia*
(Received 23 July 2010; published 16 November 2010)

The nucleation of solid Al from the melt by TiB_2 is well established and is believed to involve the formation of Al_3Ti. Since the atomic-scale mechanisms involved are not fully understood, we look to computer simulation to provide insight. As there is an absence of suitable potentials for all of this complex system we have performed large-scale density-functional-theory molecular dynamics simulations of the nucleation of solid Al from the melt on TiB_2 and Al_3Ti substrates at undercoolings of around 2 K. Using periodic boundary conditions, we find limited ordering and no signs of incipient growth in the liquid Al close to the B-terminated surface of TiB_2. By contrast, we see fcc-like ordering near the Ti-terminated surface, with growth being frustrated by the lattice mismatch between bulk Al and the TiB_2 substrate. The Al interatomic distances at the Ti-terminated surface are similar to distances found in Al_3Ti; we suggest that the layer encasing TiB_2 observed experimentally may be strained Al on a Ti-terminated surface rather than Al_3Ti. For the Al_3Ti substrate, fcc-like structures are observed on both sides which extend rapidly into the melt. Periodic boundaries introduce unphysical stresses which we removed by introducing a vacuum region to separate the liquid from the solid at one of the interfaces. We see ordering in the Al on both the B-terminated (0001) surface of TiB_2, and on $Al_3Ti(112)$, with the ordering able to be stronger on the Al_3Ti substrate. However, we cannot draw strong conclusions as these simulations need more time to allow long-ranged fluctuations in the liquid Al to dampen out. The huge computational cost restricted the range and duration of simulations that was possible.

DOI: 10.1103/PhysRevB.82.184203 PACS number(s): 81.10.Aj, 61.20.Ja, 64.60.Q−, 64.70.D−

I. INTRODUCTION

One procedure to form metal into a useful object is to melt it and pour it into a mold; the metal then cools to form a solid casting. However, the way the solid forms during cooling can have a profound effect on the mechanical properties of the resultant casting. In particular, the size of the grains that form influences the strength: for greater strength we need smaller grains. Left to itself, the growth of solid will mostly nucleate on the walls of the mold, and will grow along one axis producing columnar grains. To produce an even distribution of small grains, a refiner consisting of small solid particles is added to nucleate solid throughout the melt. The refiner also changes the shape of the grains: they have equal size in all three dimensions (3D) (equiaxed grains).

In 1951 Cibula[1] proposed that TiB_2 is an effective nucleant for primary α-Al in the melt, and now the addition of master A1-Ti-B alloys is almost universally practiced in Al alloy castings.[2] For example, A1-5 wt %Ti-1 wt %B master alloys are commercially available that contain submicron sized TiB_2 particles and a small amount of Ti solute. However, the mechanism by which it operates is still not fully understood because of the difficulties in measuring directly the nucleation kinetics at high temperature. In particular, there has been a long-running debate over the relative importance of Al_3Ti, TiB_2 and excess Ti. A number of studies[3–6] have been carried out to try to identify the mechanism of α-Al nucleation. Mohanty and Gruzleski[7] designed an experiment to directly add TiB_2 refiner using an inert gas stream; this enabled them to study the effect of the refiner on grain size during Al-Si alloy solidification. Using a combination of optical microscopy, scanning electron microscopy and an electron probe microanalyzer, they found that TiB_2 was pushed into the region between α-Al dendrites if no Ti was added, and that Al_3Ti layers were absent, suggesting that TiB_2 alone does not nucleate α-Al. On the other hand, they reported the presence of blocky Al_3Ti crystals in the center of each grain when both TiB_2 and solute Ti are present. Schumacher and Greer[8] performed the first experiment to identify the nucleation agents for α-Al using high-resolution transmission electron microscopy. They added an A1-Ti-B alloy to molten $Al_{85}Ni_5Y_8Co_2$, which they then rapidly quenched to form a glass, which can be considered an analog of a liquid. The quench stopped the growth of solid Al, preventing it from obscuring the part of the system involved in nucleation. They were then able to observe the absorption of Ti onto TiB_2 to form layers, which they believed to be Al_3Ti, on which Al crystals then grew.[8] Their study provides direct evidence for the existence of layers which they state is Al_3Ti on top of TiB_2 prior to the nucleation of α-Al, and initiated subsequent experimental work[9] to identify the crystal orientation relationships between those phases. Recently, Inqbal *et al.*[10–12] carried out *in situ* x-ray diffraction experiments on pure Al with different volume fractions of TiB_2 inoculants and Ti solute concentrations using a synchrotron x-ray source. They successfully identified the formation of a metastable phase prior to the formation of solid α-Al, which they identified as Al_3Ti on the TiB_2. This gives strong support to the observation of Schumacher and Greer[8] that the nucleation of Al on TiB_2 requires a precursor layer of Al_3Ti.

A full atomistic understanding of the nucleation mechanism is difficult to obtain from experiment, so we have turned to computer simulations to identify the events that occur. Since there is no set of suitable potentials that span Al,

TABLE I. Systems and boundary conditions used in simulations.

Simulation	System	T (K)	B.C.	No. of planes in Al_3Ti or TiB_2	No. of Al_3Ti or TiB_2 units	No. of liquid Al atoms
TiB_2AlP	$Al(111)\|\|TiB_2(0001)$	910	P	$8_{[1000]}\times 12_{[11\bar{2}0]}\times 4_{[0001]}$	32	160
Al_3TiAlP	$Al(111)\|\|Al_3Ti(112)$	910	P	$12_{[110]}\times 8_{[11\bar{2}]}\times 6_{[112]}$	144	144
TiB_2AlF	$Al(111)\|\|TiB_2(0001)$	910	F	$8_{[1000]}\times 12_{[11\bar{2}0]}\times 4_{[0001]}$	32	160
Al_3TiAlF	$Al(111)\|\|Al_3Ti(112)$	910	F	$12_{[110]}\times 8_{[11\bar{2}]}\times 6_{[112]}$	144	144

Ti, and B we have used density-functional theory (DFT) to provide a robust description of the forces between the atoms. Because of recent advances in parallel computers and the development of efficient DFT computer codes, we have been able to perform molecular dynamics (MD) to simulate the nucleation of solid Al from the melt by Al_3Ti and TiB_2 substrates. We find that Al_3Ti is indeed a good nucleating material but also find that the precursor layer observed on TiB_2 could be strained Al on a Ti-terminated face rather than Al_3Ti.

II. METHODOLOGY

A. Simulation software

The calculations were performed with the Vienna *ab initio* simulation package (VASP).[13–16] In this code, a plane-wave basis set for the expansion of the wave functions is used. The rapid oscillations in the wave functions are treated using projector-augmented waves (PAWs),[17,18] and the contribution to the energy from electronic exchange and correlation is described using the PW91[19,20] gradient-corrected density functional. Performance is improved through the use of an efficient second-order extrapolation of the charge density, parallel 3D fast Fourier transforms, and the mixed block Davidson method[21] plus a residual minimization scheme using direct inversion in the iterative subspace[22] for wave-function optimization. An energy tolerance of 10^{-4} eV/atom was used as a test of charge self-consistency. The plane-wave cutoffs for liquid Al/TiB_2 and liquid Al/Al_3Ti were 536 eV and 329 eV, respectively. The simulations were performed with a $2\times2\times1$ k-point mesh.

B. Systems and conditions

Two substrates [$Al_3Ti(112)$ and TiB_2 (0001)] were considered, as shown in Table I. To establish the correct cell sizes we constructed two cells: one of perfect crystalline Al_3Ti (in the $D0_{22}$) structure in contact with fcc Al forming an $Al(111)\|Al_3Ti(112)$ interface; the other of perfect hcp TiB_2 in contact with fcc Al forming an $Al(111)\|TiB_2$ (0001) interface. The lattice parameters were $a=b=3.85$ Å, and $c=8.58$ Å for Al_3Ti (Ref. 23) and $a=b=3.03$ Å and $c=3.23$ Å for TiB_2.[24] The Al_3Ti region contains $12\times8\times6$ atomic layers and the TiB_2 region has $8\times12\times4$ layers. To generate the starting coordinates for the liquid Al we removed the substrate material (TiB_2 or Al_3Ti) and performed MD at 1273 K and an average pressure of 0 Pa using an Embedded Atom Method (EAM) potential[25] and the Hoover NVT ensemble[26] as implemented in LAMMPS.[27] To ensure that the liquid Al had zero pressure after being reunited with its substrate, the computational cell was stretched slightly before adding the substrate back in. We believe the number of atoms used for the substrates and the liquid Al is adequate for obtaining useful information about nucleation: the substrates retain their solid structure, and the pair correlation function in the liquid region shows the system is disordered. Larger numbers of atoms are desirable, but unaffordable. Periodic boundary conditions were applied in the x and y directions. In the z direction periodic boundary conditions (PBCs) were used, but for one set of simulations there is no vacuum present (symbol P), while for the other set a vacuum region was inserted on top of the liquid Al (symbol F): see Table I.

We performed two types of simulation: one consisting of 160 liquid Al atoms on top of 32 TiB_2 units, the other with 144 liquid Al atoms combined with 144 Al_3Ti units. Using the reference melting point (912 K) calculated by Alfè *et al.*[28] using VASP with PAW and generalized gradient approximation (GGA), we studied α-Al nucleation at small undercoolings (~2 K). The MD simulations were all performed at constant temperature (~910 K) in the NVT ensemble, with a time step of 1 fs. We ran the simulations for between 2.0 and 2.85 ps in order to observe the ordering in the liquid Al close to the substrates.

C. Simulation hardware

The simulation of TiB_2 with liquid Al using periodic boundary conditions was performed on an IBM Blue Gene/L computer at Blue Gene Watson (BGW) in the IBM's Thomas J. Watson Research Center in Yorktown Heights, NY, USA. In total, 128 nodes (256 cores) were used, with each node containing two 700 MHz power 440 dual core processors and 512 MB of memory. The remaining simulations were carried out on a 16-rack IBM Blue Gene/P system in the Supercomputing Laboratory (KSL) at the King Abdullah University of Science and Technology (KAUST): each node has four 850 MHz PowerPC 450 quad core processors and 4 GB of memory.

To allow us to make efficient use of the parallel computing resources, we first tested the scaling of the code with respect to the number of nodes on the KSL Blue Gene/P system using the TiB_2AlP system (see Table I). We used parallelization over bands and plane-wave coefficients. The measured speedup is shown in Fig. 1, where we have defined the speedup to be $16\times t_{16\ \mathrm{cores}}/t_{n\ \mathrm{cores}}$, and $t_{16\ \mathrm{cores}}$ and $t_{n\ \mathrm{cores}}$

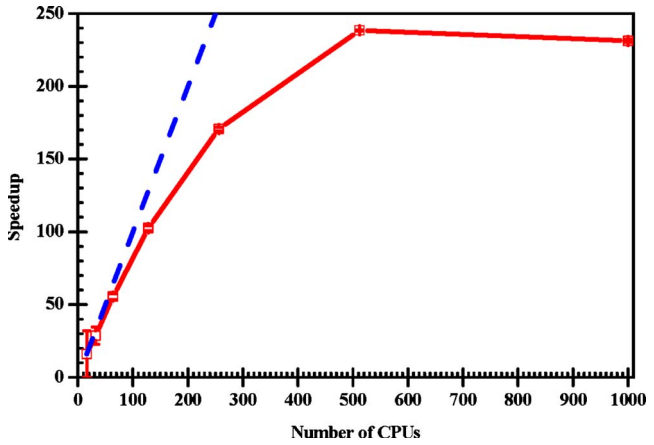

FIG. 1. (Color online) The simulation time for single step of ionic relaxation of TiB_2AlP system as a function of number of cores used on IBM Blue Gene, KSL, KAUST.

are the times to perform the calculation using 16 cores and n cores, respectively. For an ideal system the speedup should equal n. From Fig. 1, we see that speedup is useful up to 256 cores but falls off after that with no additional speedup if over 512 cores are used: this is plausible as our TiB_2AlP simulations contain only 256 atoms. We used 256 cores for all of our simulations.

D. Analysis of density profile

The results of our simulations have been analyzed by inspecting the density profile ($\rho(z)$) averaged over slices of the cell parallel to the solid/liquid (S/L) interface calculated using the following formula:[29,30]

$$\rho(z) = \frac{\langle N_z \rangle}{A_{xy}\Delta z}, \tag{1}$$

where $\langle N_z \rangle$ is the time averaged number of atoms in a bin of size Δz at z, and A_{xy} is the area of the S/L interface. The resulting profile is sensitive to the choice of bin size (Δz); to obtain a good spatial density distribution, the density fluctuations inside a bin have to be much smaller than the variation in the density between neighboring bins. In these calculations the number of bins was set at 300 (equivalent to a bin size of 0.11 Å), and the time average was taken over 50 snapshots separated by 0.05 ps. While this averaging time is less than a typical vibrational period (0.1–1 ps) it was kept this short to avoid averaging over the ordering events we are trying to observe.

E. Quantification of structural ordering

Because nucleation involves a transition from disordered liquid to ordered solid, a measure of the local ordering at the S/L interface is a very informative tool for interpreting the evolution of the interface. Many authors have proposed methods to characterize the short-range structural ordering during solidification, including the common neighbor analysis,[31] the centrosymmetry parameter (CSP),[32] the common neighborhood parameter,[33] and the ordering discriminator function.[34] We choose to use the CSP, as it is easiest to interpret. It gives a measure of how far a structure is from being centrosymmetric, with large values indicating large departures. Not only can liquid and solid be effectively distinguished using this parameter but also defect sites in the Al_3Ti substrate. For an fcc structure the CSP is defined as[32]

$$\alpha = \sum_{i=1,6} |R_i + R_{i+6}|^2, \tag{2}$$

where R_i and R_{i+6} are bond vectors corresponding to the six pairs of opposite nearest neighbors, and the nearest neighbors are identified by finding the opposite atoms closest to the positions defined by the undistorted nearest-neighbor vectors. For bulk Al in the fcc structure, $\alpha=0$, for the (001) surface $\alpha=24.9$ Å^2, for an intrinsic stacking fault $\alpha=8.3$ Å^2, for atoms midway between fcc and hcp $\alpha=2.1$ Å^2, and for liquid atoms with disordered structure $16<\alpha<24.9$ Å^2.[33]

Buta *et al.*[30] proposed a quantity that can measure both long- and short-ranged lateral order, namely the two-dimensional (2D) structure factor $S_{2D}(k)$,[35]

$$S_{2D}(k) = \frac{1}{N}\sum_{i,j}^{N} \langle \exp i\vec{k}\cdot(\vec{r}_i - \vec{r}_j)\rangle$$
$$= \frac{1}{N}\sum_{i,j}^{N} \cos[k_x(x_i - x_j) + k_y(y_i - y_j)]. \tag{3}$$

This two-dimensional representation of the layer structure generates a periodic pattern similar to x-ray or neutron-scattering experiments: it gives the Fourier components of in-plane density fluctuations in the liquid computed from projections of the atomic positions onto the plane of the interface. This analysis allows us to identify lateral ordering within the interfacial layers on top of the $TiB_2(0001)$ and Al_3Ti (112) substrates.

III. RESULTS AND DISCUSSION

A. TiB_2 substrate

Using PBCs, the Al_3TiAlP simulation was performed at a temperature of 910 K, roughly corresponding to an undercooling of 2 K. (Note that the small cell size means that there will be a rise in the temperature at which the liquid is stable,[36] so the effective undercooling is greater than this.) There are two kinds of (0001) interface for the TiB_2 crystal: Ti-terminated and B-terminated. We intentionally add two Ti atoms to the liquid Al, with one in the bulk and the other next to the B terminated S/L interface. The purpose was to observe any effect from low concentrations of solute Ti.

In Fig. 2, three typical snapshots of liquid Al on top of TiB_2 at 910 K are shown together with the corresponding density profiles, $\rho(z)$, averaged over a period of 0.05 ps. The TiB_2 region has two Ti planes and two B planes, producing one Ti-terminated surface and one B-terminated surface. This is then surrounded by liquid Al atoms at the beginning of the simulation [Fig. 2(a)]. The calculated density profile perpendicular to the S/L interface shows the Ti (magenta dotted

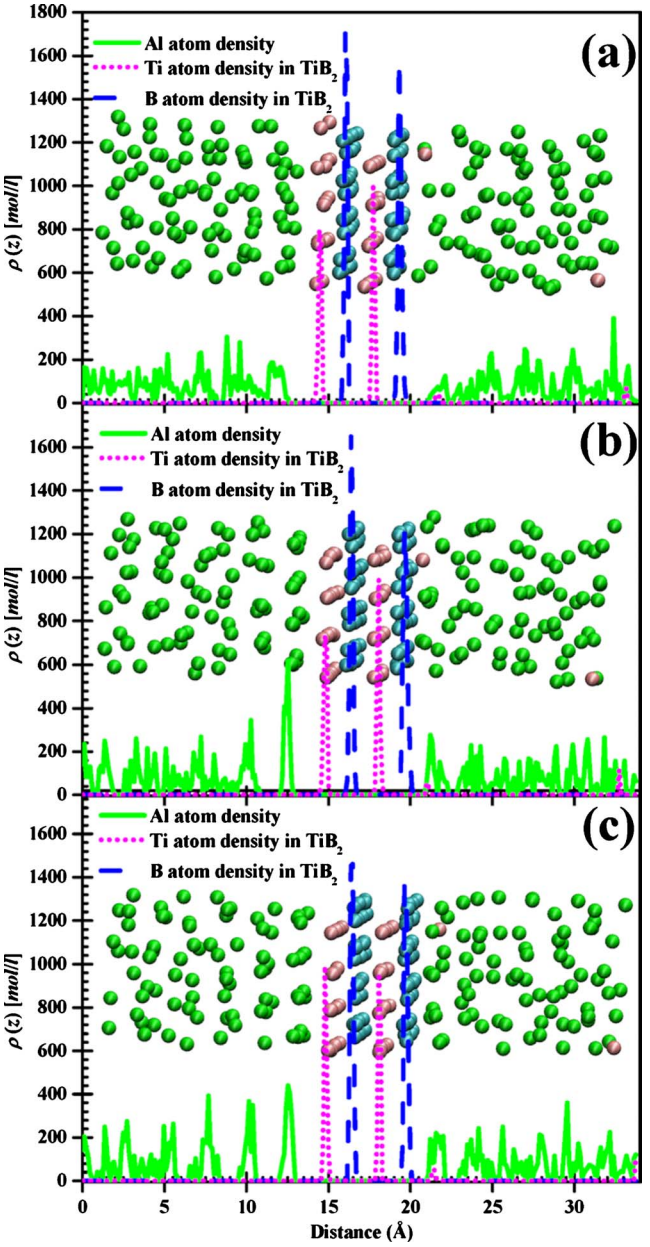

FIG. 2. (Color online) Sequential images and calculated density profile of solid Al nucleation from the melt on top of TiB_2 substrate at $T=910$ K using periodic boundary condition. (a) $t_s=0.05$ ps; (b) $t_s=1.42$ ps; (c) $t_s=2.85$ ps.

lines) and B (blue dashed lines) planes, in contrast to the random positions of the Al (green straight lines) atoms in the liquid. However, ordered structure is visible in the liquid Al by 1.42 ps [Fig. 2(b)]. Solidlike structural ordering is initiated in the first liquid layer on top of the TiB_2 substrate, and then propagates outward into the bulk liquid. However, the ordering is different on the B- and Ti-terminated surfaces. On the B-terminated surface only one Al ordered layer forms, which is followed by another layer that is quite disordered. On the Ti-terminated surface the ordering extends three or more layers into the liquid [see Fig. 2(c)]. In both cases the density oscillations dampen gradually from the S/L interface to a uniform distribution when liquid phase dominates.

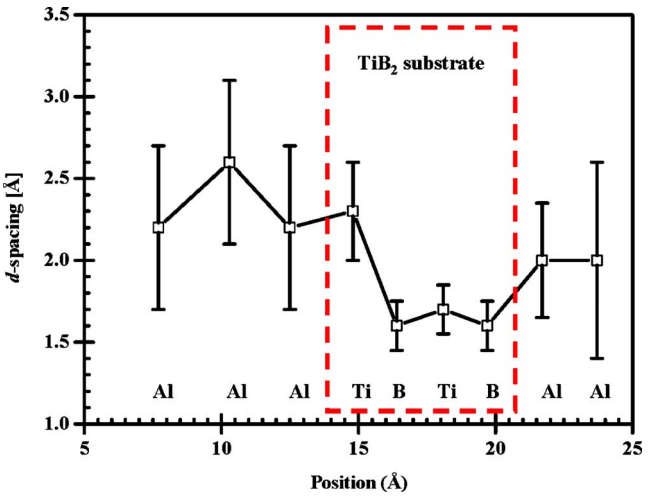

FIG. 3. (Color online) d spacing as a function of atomic position. A bin size of 0.11 Å was used to build the histogram from which the peak positions were found. The error bars are found from the half width at half maximum of the peaks.

Using a bin size of 0.11 Å, we calculated the distribution of interplanar spacing (d spacing) normal to the S/L interface, as shown in Fig. 3. The d spacing at position z is defined as the distance between the peak at z and the first peak to its left. First we note the interplanar spacing within the TiB_2 substrate is constant (1.6 ± 0.15 Å) and very similar to the bulk value of 1.62 Å (see Table II), confirming that our thin slab is sufficient for this simulation. Two different interplanar spacings are observed in the peak positions of the ordered Al layers. On the right-hand side (B-terminated surface), the Al atoms are situated at the same positions that Ti would occupy in the TiB_2 structure, giving an AlB_2 crystal structure with an interplanar spacing of 1.9 ± 0.4 Å. This is expanded by about 25% compared with the bulk value of 1.63 Å (see Table II); the reason for this is probably that the structure cannot grow further, so the solidlike Al region is strongly perturbed by the neighboring liquid Al. However, this needs further analysis and will be examined in more detail in future work. Presumably it is the absence of B that inhibits growth beyond about one ordered layer plus one

TABLE II. Lattice constants, neighbor distances, and interplanar spacings for key structures.

	Lattice parameters		Neighbor distances		Interplanar spacing	
	a,b (Å)	c (Å)	r_{1nn} (Å)	r_{2nn} (Å)	Index	d (Å)
Al[a]	4.05	4.05	2.86	4.05	(111)	2.34
Al_3Ti [b]	3.85	8.58	2.72	3.85	(112)	2.31
TiB_2 [c]	3.03	3.23	3.03 (Ti-Ti)		(0001)	1.62
AlB_2 [d]	3.01	3.25	3.01 (Al-Al)		(0001)	1.63

[a]Reference 37.
[b]Reference 23.
[c]Reference 24.
[d]Reference 38.

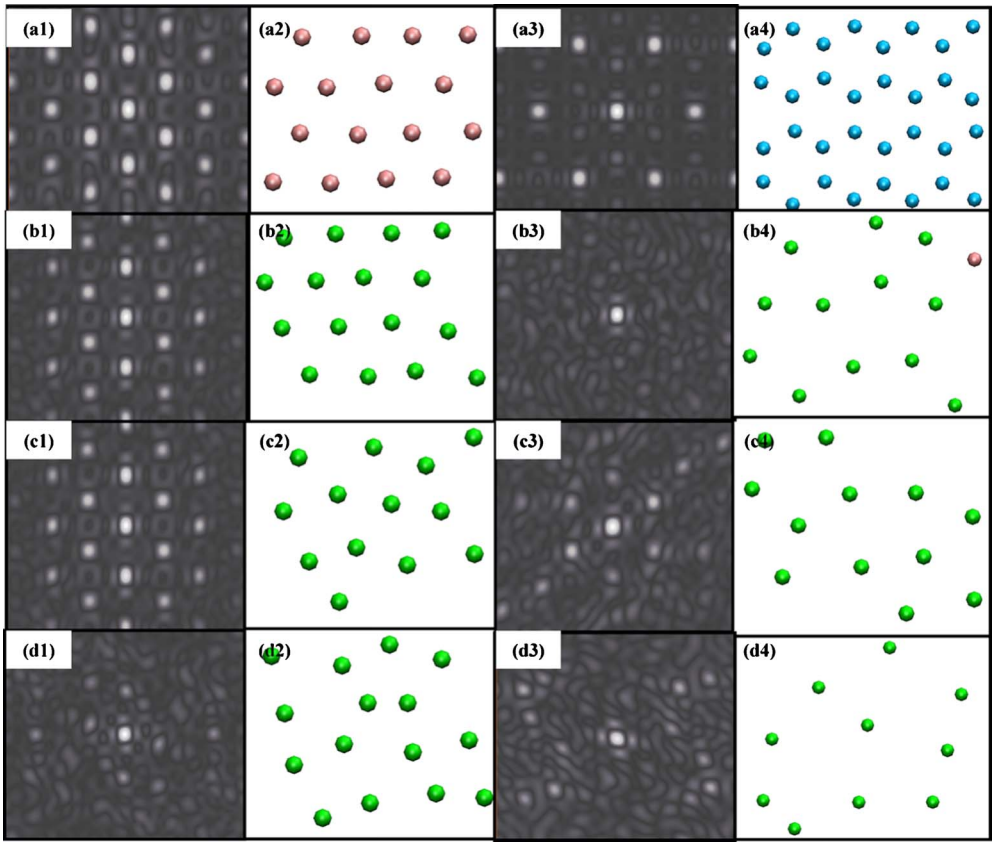

FIG. 4. (Color online) Two-dimensional structure factor and corresponding ordering layers on the Ti side [(a1) and (a2)] and B side [(a3) and (a4)] of TiB2. [(a1) and (a2)] Ti layer; [(a3) and (a4)] B layer, [(b1)–(b4)] first layer in the liquid Al; [(c1)–(c4)] second layer in the liquid Al; [(d1)–(d4)] third layer in the liquid Al. Computed at $t=2.85$ ps

disordered layer. On the left-hand side (Ti-terminated surface) an fcc-like structure with an interplanar spacing of about 2.4 ± 0.5 Å is nucleated in the liquid and extends into the liquid for at least three layers. This d spacing is very similar to the room temperature experimental interplanar spacing of Al (111)[39] of 2.34 Å (see Table II).

Precisely what would happen if the simulation were run longer is unclear. It took 1 month to complete 2.85 ps for the TiB_2AlP system of, and we are currently unable to take this further. However, one message is clear: Al grows much more readily on the Ti-terminated surface than on the B-terminated one.

In order to compare the ordering as a function of distance away from the two types of substrate surfaces (Ti- and B-terminated TiB_2), we calculated the two-dimensional structural factor at time $t=2.85$ ps as shown in Fig. 4 Hexagonal patterns are observed on both surfaces. Figure 4b2 confirms that Al forms (111) fcc planes on the Ti-terminated surface while on the B-terminated surface Fig. 4b4 shows that the Al atoms roughly occupy the Ti sites of the TiB_2 structure.

Using the three layers of atoms on the Ti-terminated surface shown in Figs. 4b2–4d2, and the three layers on the B-terminated surface shown in Figs. 4b4–4d4, we calculated the radial distribution function (RDF) of Al-Al pairs on both sides of the TiB_2 substrate as shown in Fig. 5(a). The RDF for the Ti-Ti, Ti-B, and B-B pairs in the TiB_2 substrate were also obtained, together with the RDF of Al-Al pairs in the bulk liquid (excluding the six layers close to TiB_2 substrate). No ordering beyond the first neighbor shell is observed in the bulk liquid or near the B-terminated surface. Structural ordering out to about the third neighbor shell is seen in the first three Al layers near the Ti-terminated surface, with strong peaks appearing at 2.75 and 3.85 Å. These correspond well to two neighbor separations in the $D0_{22}$ Al_3Ti structure (2.72 and 3.85 Å), which might explain the apparent presence of Al_3Ti in the experimental x-ray spectra.[10–12]

There is also a weaker peak at 3.25 Å, whose significance is as follows. A surprising feature of the nearest-neighbor distance (2.75 Å) is that it is 4% smaller than the bulk room-temperature spacing of 2.86 Å while the effective lattice constant (measured by the interplanar spacing and the substrate lattice constants) is rather similar to that for the room temperature solid on the Ti surface. We credit this to the dynamics of the Al atoms being captured in the pair-correlation function in a different way than in the average one-dimensional density. The two can be seen to be compatible as the longer distance (3.25 Å), when averaged with the shorter distance (2.75 Å) gives an average (3.00 Å) very similar to the Ti-Ti distance (3.03 Å) in the substrate, which we expect to define the average in-plane Al-Al distance. On the B-terminated surface, the RDF for Al-Al only has clear peaks at 2.75 and 3.05 Å, matching both the first neighbor in liquid Al and the first neighbor in AlB_2 (the liquid Al forms

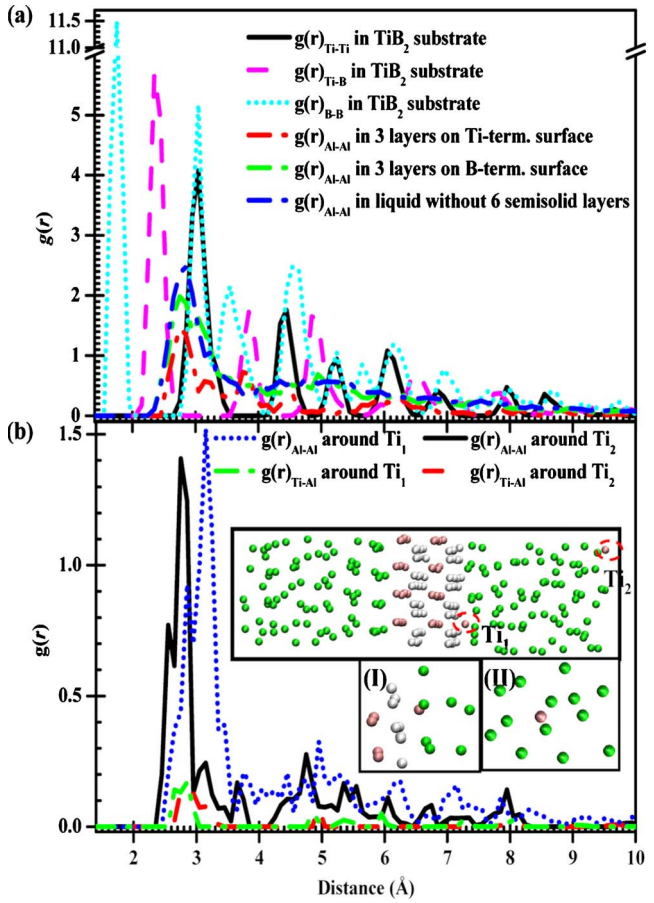

FIG. 5. (Color online) (a) The RDF of Ti-Ti, Ti-B, B-B in the solid substrate and Al-Al in the solidlike films on both sides of TiB_2 and the bulk liquid which are calculated from the last 100 MD steps at 910 K. (b) The RDF of Al-Al and Ti-Al around the Ti atoms in the liquid with insert images (I and II) showing different ordering behaviors of atoms around Ti atoms.

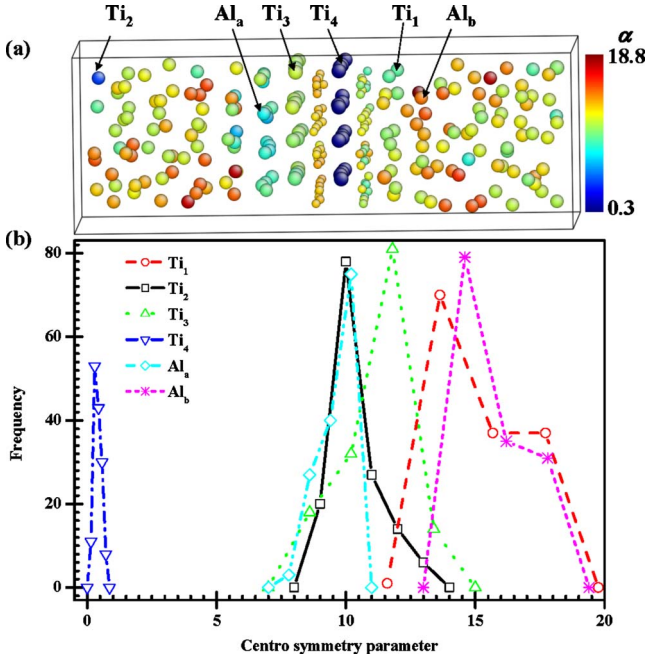

FIG. 6. (Color online) (a) The atoms colorized by their averaged centro symmetry parameter (α) over the last 200 fs showing the ordering of Al atoms on the Ti-terminated surface (Al_a), disordered liquid Al (Al_b), three different positions of Ti atoms including a single Ti atom on the B-terminated surface (Ti_1), in bulk liquid (Ti_2), at the surface of the TiB_2 substrate (Ti_3), and in the middle of the TiB_2 substrate (Ti_4). (b) The distribution of α for each atom type.

a thin film of AlB_2 on top of TiB_2). In the substrate, the RDF of Ti-Ti pairs has five peaks at 3.05, 4.45, 5.25, 6.05, and 6.85 Å within the cutoff of 10.0 Å, and four nearest neighbors were identified for Ti-B pair which were at distances of 2.35, 3.85, 4.85, and 6.55 Å.

We now investigate the ordering of atoms around the two added Ti atoms [Ti_1 and Ti_2 in the inset images in Fig. 5(b)]. We calculated the RDF for the first layer of liquid on top of the B-terminated TiB_2 surface and 12 Al atoms around the Ti_2 atom in the bulk liquid, as shown in Fig. 5(b). The first peak of $g(r)_{\text{Al-Al}}$ in the first layer of liquid on the B-terminated TiB_2 surface is at a distance of 2.85 Å, close to the second neighbor Al-Al distance of 2.88 Å in Al_3Ti while the second peak is at 3.15 Å, which is close to the Al-Al distance in AlB_2. It might be that the presence of Ti is inhibiting the formation of the AlB_2 thin film by promoting the formation of an Al_3Ti, which might also explain why the 2D structure factor in Fig. 4b3 is not as clear as the second layer in Fig. 4c3. From Fig. 5(b) we see that $g(r)_{\text{Al-Al}}$ around Ti_2 has three peaks at 2.75, 3.65, and 4.75 Å, while $g(r)_{\text{Ti-Al}}$ around Ti_2 exhibits three peaks at 2.75, 3.25, and 4.95 Å. These do not match exactly separations in the Al_3Ti structure but are quite close.

In addition to the pair distribution function, we also quantified the centro symmetry parameter (α) distribution for each atom over the last 200 fs of simulation [Fig. 6(a)] with the color showing the averaged degree of ordering. This parameter is close to zero for an fcc crystal and is greater than 16 when the atoms are in a disordered state such as liquid. Clearly, the Al atoms on top of the Ti-terminated surface tend to form several ordered layers. The degree of ordering on the B-terminated surface decreases dramatically as it moves from the first layer into the liquid. Interestingly, four different z positions of Ti atoms show completely different degrees of ordering (compare Ti_1-Ti_4 in Fig. 6). We plotted the distribution of ordering over this period in Fig. 6(b). Ti_1 is slightly less ordered compared to the liquid Al_b atoms because the mean α value is smaller. Surprisingly, Ti_2 shows the same degree of ordering as the Al atoms (Al_a) on top of the Ti-terminated surface of TiB_2. This means that Ti_2 promotes the surrounding atoms to form an fcc structure inside the bulk liquid. Atoms at the Ti-terminated surface (Ti_3) are more disordered as compared to the Ti atoms in the middle of the TiB_2 substrate (Ti_4). However, this degeneration of ordering has successfully transferred ordering from the Ti substrate into the liquid Al gradually. This analysis of the structural ordering observed on $Al_{a,b}$, and Ti_{1-4} thus supports the experimental findings that formation of an fcc-like structure is promoted by the presence of Ti atoms.[3–6]

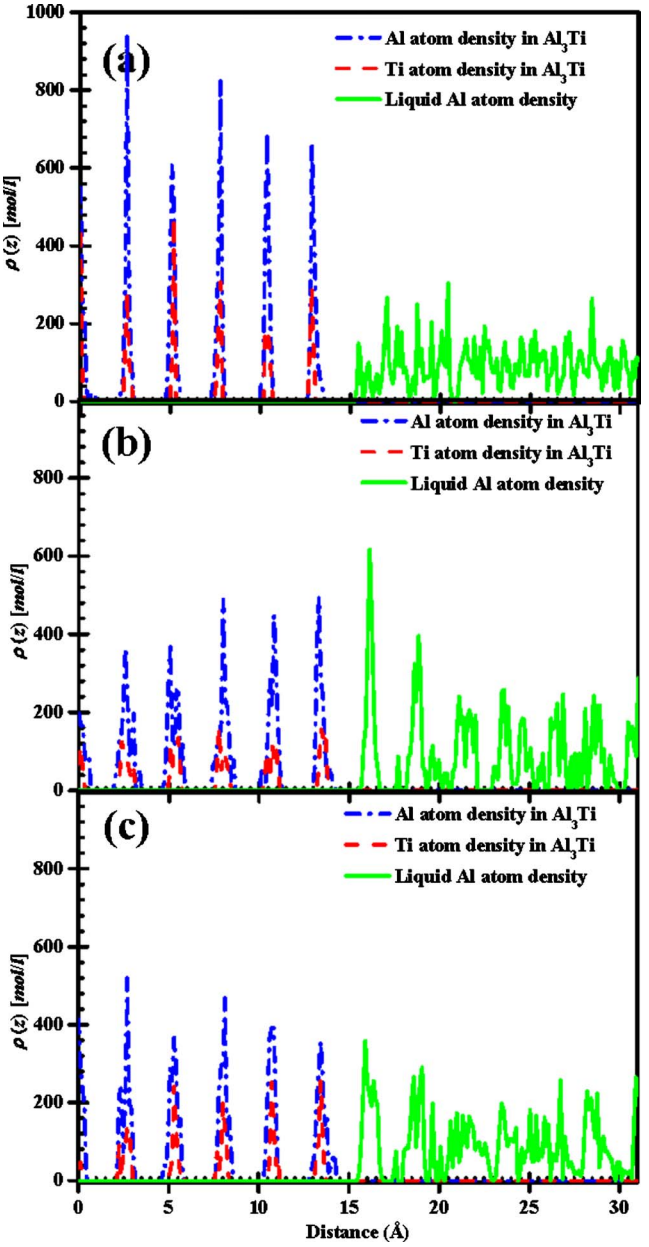

FIG. 7. (Color online) Calculated density profile of solid Al nucleation from the melt on top of the Al_3Ti substrate at $T=910$ K using periodic boundary condition. (a) $t_s=0.05$ ps; (b) $t_s=1$ ps; (c) $t_s=2$ ps.

B. Al_3Ti substrate

As for the TiB_2AlP simulation, we performed *ab initio* MD at 910 K using an *NVT* ensemble in a system (Al_3TiAlP) containing both a solid slab of Al_3Ti and liquid Al; the solid substrate forms an interface with the liquid at its (112) surfaces on both sides. The Al_3Ti structure has no compositional variation between the two (112) surfaces. The time to complete a 2 ps simulation with 288 atoms was one month on 256 cores. We obtained 2000 atomic configurations which were then analyzed by calculating the density profile along the direction perpendicular to the S/L interface. The resulting plots of Al and Ti atom densities in the Al_3Ti substrate and the Al atom density in the liquid are shown in Fig. 7.

The interplanar spacing for the Al_3Ti substrate retained its bulk value, just as we saw for the TiB_2 structure. In contrast to the TiB_2 substrate shown in Fig. 2, fcc-like structural ordering is initiated and propagates into the liquid on both sides of the Al_3Ti substrate as shown by the structuring of the liquid Al density profile after only 1 ps [Figs. 7(a) and 7(b)]. There are periodic oscillations in the density of the substrate corresponding to (112) planes of atoms [Ti (red) and Al (blue)], and their d spacing is 2.34 Å initially, expanding to 2.68 Å after heating to 910 K. After holding the liquid Al on both sides of the Al_3Ti substrate for 1 ps, the maximum density of the first ordering layer (308 mol/l) on top of the Al_3Ti substrate in Fig. 7(b) almost reaches the same value as the sum of the densities for Al and Ti in the substrate (363 mol/l). The ordering phase has the same interplanar spacing as the Al_3Ti substrate. A longer holding time allows more solid phase to grow on both sides, and when the two solid phases meet in the middle, stress is created as they are not perfectly registered. From Figs. 7(c) and 7(b), we see that this leads a new loss of order.

In order to observe how the ordering extends into the liquid we calculated the 2D structure factor using Eq. 8. As shown in Fig. 8(a), the snapshot of the last configuration clearly shows ordering in the first three layers on top of Al_3Ti substrate. Using the outmost layer of the Al_3Ti structure [Fig. 8d1] and the three liquid Al layers closest to it [Figs. 8a1–8c1], we calculated a 2D structure factor for each slice, as shown in Figs. 8a2–8d2. The structure of the atoms in the first layer [Fig. 8c2] matches that of the Al_3Ti substrate [Fig. 8d2] while the ordering decays as we move further into the liquid, as shown in Figs. 8a2 and 8b2. It is clear that liquid Al forms an fcc structure with a lattice constant similar to that for Al_3Ti. This might explain why Al_3Ti is a powerful nucleant that easily initiates the formation of fcc Al solid from the melt.

C. Comparison of the B-terminated TiB_2 and Al_3Ti (112) surface

For both TiB_2AlP and Al_3TiAlP we calculated the initial pressure and final pressure. We found positive pressures (about 5.0×10^8 Pa) at the beginning and negative pressures (about -3.0×10^9 Pa) at the end of the simulations; these are both uncomfortably large, and might help explain the large Al interplanar spacing on the B surface of TiB_2. In order to make a better comparison of the relative effectiveness of Al_3Ti and TiB_2 in nucleating solid Al from the melt we need to eliminate these stresses. Their origin is the interaction between the two growing ordered regions produced by the periodic boundaries. The sharp change in pressure occurs because solid Al nucleates on both sides of the substrates, and the whole system contracts to accommodate the solidification shrinkage. One approach might be to use constant pressure (*NPT*) MD instead of constant volume (*NVT*) MD. However, our version of VASP does not provide this feature. Instead we add a vacuum region on top of the liquid, keeping only one interface in each system, thereby allowing stress to be released along the direction perpendicular to the interface. Using this methodology the TiB_2AlF and Al_3TiAlF systems

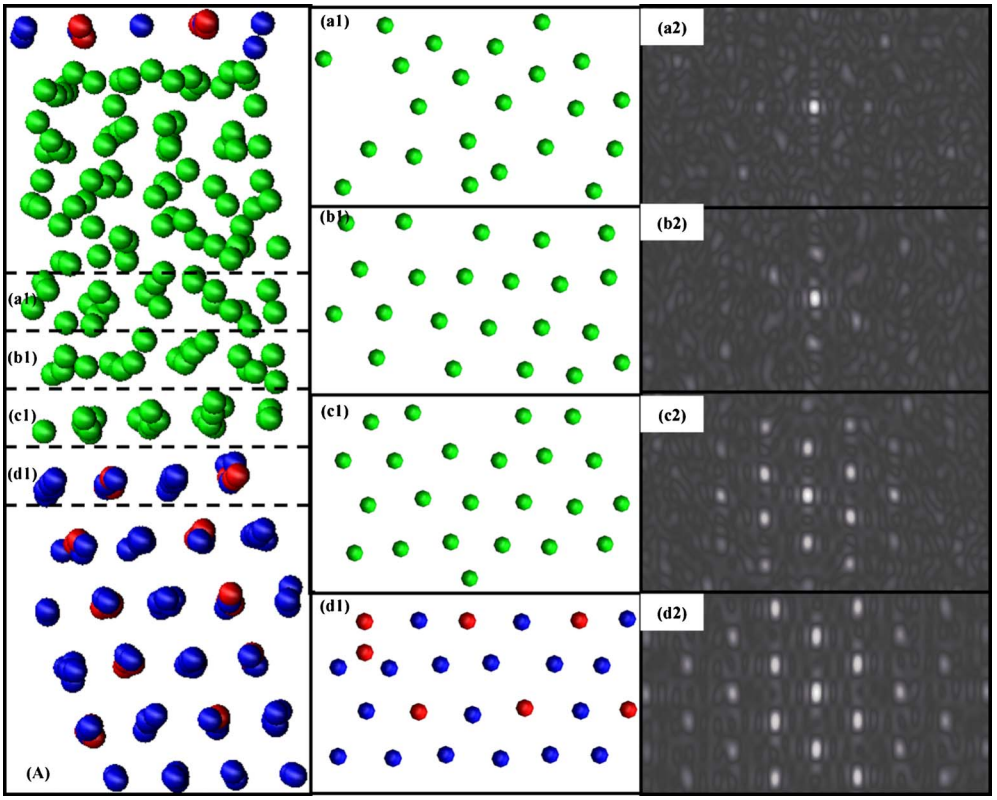

FIG. 8. (Color online) Structural ordering at the beginning of continuous growth on Al_3Ti (112) surface at 910 K. (a) a snapshot at $t_s=2$ ps, and projections of the outer four layers [(a1)–(d1)] and the corresponding time-averaged structure factors for 50 MD steps [(a2)–(d2)]. Ti and Al atoms in Al_3Ti structure are in red (gray) and blue (dark), respectively. Liquid Al atoms are in green (light gray).

were simulated to compare the efficiency with which TiB_2 and Al_3Ti nucleate solid Al from the melt.

The density profiles, $\rho(z)$, computed at three times (0.05, 1, and 2 ps) and averaged over a period of 0.05 ps for a simulation at 910 K, are shown in Fig. 9. They reveal structural ordering on top of both the $TiB_2(0001)$ basal plane and the $Al_3Ti(112)$ surface. Three typical snapshots of the atomic positions are also shown for these times. Because there is a vacuum region separating the liquid Al and Ti-terminated surface of TiB_2, solid Al can only nucleate from the melt on top of the B-terminated TiB_2 surface. At the beginning of the simulation a disordered phase is clearly seen from the random oscillations in the density profile [Fig. 9(a)]. After 1 ps solid films start forming on top of the B layer in the TiB_2 substrate as seen in Fig. 9(b). The d spacing was measured to be 1.79 Å, a bit larger than the interplanar spacing of the AlB_2 structure of 1.63 Å at room temperature due to thermal expansion at high temperature. After 2 ps, a second solid layer is stabilized, with an interlayer spacing of 2.12 Å.

The liquid Al on top of $Al_3Ti(112)$ orders rapidly within 1 s, with ordering extending over several layers as shown by comparing Figs. 9(d) and 9(e). However, this order is transient, as can be seen by comparing Figs. 9(e) and 9(f). We hypothesize that this is because there are long-range fluctuations in the liquid Al that take time to dampen out. In order to obtain an estimate of the total time required to reach a stable configuration we performed classical molecular dynamics using an empirical potential derived from the embedded atom method for the Al-Ti system.[25] Using the same conditions and configuration (Al_3TiAlF), we found that continuous growth of solid Al on $Al_3Ti(112)$ occurs after 7.5 ps and complete solidification occurs within 14.5 ps. Therefore, more simulation time must be allowed if the optimal configuration for continuous growth is to be obtained by relaxation for Al_3TiAlF system.

Our preliminary TiB_2AlF and Al_3TiAlF calculations, which each took 1 month on 256 cores, provide us with qualitative information about the effectiveness of two different substrates for nucleating solid Al from the melt. Only two to three ordering layers ever appeared on the B-terminated surface of TiB_2 [see Fig. 9(c)] and it does not display the fluctuations in order seen in the liquid on the $Al_3Ti(112)$ substrate [see Fig. 9(f)]. In addition, the *d* spacing in the new solid phases differ on the two kinds of substrate. Liquid Al on $Al_3Ti(112)$ forms close-packed (111) planes of fcc structure with an interlayer spacing of about 2.74 Å. Therefore, α-Al appears to nucleate much more readily on $Al_3Ti(112)$ than on the B-terminated TiB_2 (0001) basal plane, though we cannot draw strong conclusions from these short simulations.

IV. SUMMARY AND CONCLUSION

We have investigated heterogeneous nucleation of α-Al from the Al melt upon cooling by means of *ab initio* molecular dynamics simulations (PAW with GGA as implemented in VASP). By calculating the density profile at negligible under-

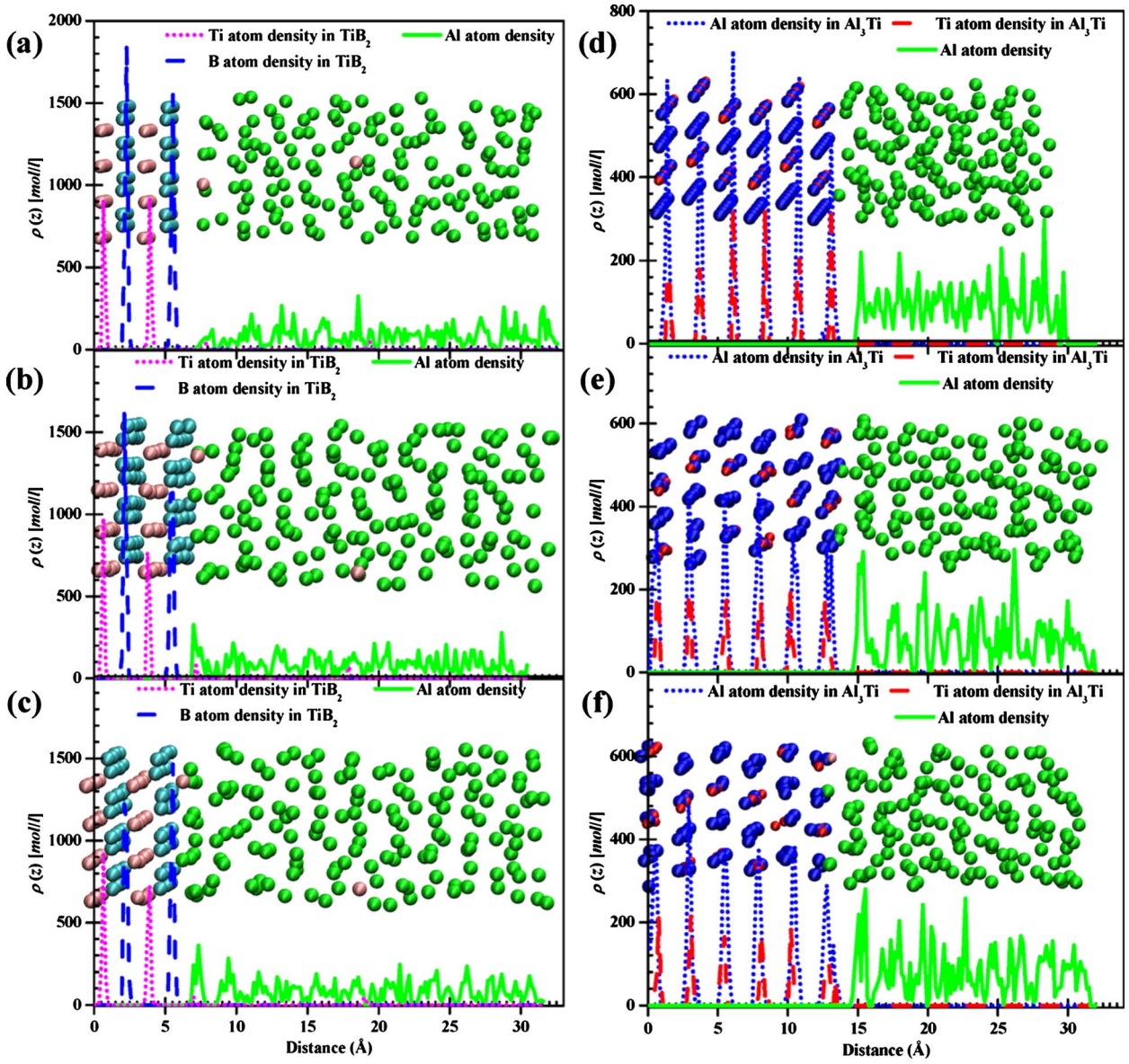

FIG. 9. (Color online) Sequential images and calculated density profile of solid Al nucleation from the melt on top of TiB_2 and Al_3Ti substrates at $T=910$ K using the free surface condition. (a) TiB_2 substrate, $t_s=0.05$ ps; (b) TiB_2 substrate, $t_s=1$ ps (c) TiB_2 substrate, $t_s=2$ ps, (d) Al_3Ti substrate, $t_s=0.05$ ps; (e) Al_3Ti substrate, $t_s=1$ ps; (f) Al_3Ti substrate, $t_s=2$ ps.

coolings (~2 K) on different kinds of substrates including Al_3Ti and TiB_2, we have successfully obtained quantitative information of heterogeneous nucleation mechanism of α-Al from the Al melt. Structural ordering was clearly seen in the liquid close to the TiB_2 and Al_3Ti substrates at temperatures below the Al melting point. Lattice parameters differ on two kinds of termination surfaces of TiB_2, promoting new structure ordering with different potentials to grow.[29] The liquid→solid transformation process on top of the B-terminated (0001) basal plane of TiB_2 does not promote fcc-like ordering, instead it tries to form an AlB_2 structure to replicate the TiB_2 lattice. The Ti-terminated surface has greater potential to nucleate α-Al, but did not promote continuous growth of Al (111) in 2.85 ps: this is probably due to the strain energy associated with the lattice mismatch between fcc Al and TiB_2. At small undercooling, liquid Al close to the Al_3Ti (112) substrate readily transforms into a solid fcc-like structure.

Interestingly, arbitrary stresses introduced by the interaction between the two ordered regions under periodic boundary conditions prevent complete solidification. We found that these artificial forces can be removed by inserting a vacuum region on top of the liquid. However, the computational cost to reach complete solidification for Al_3TiAlF (as estimated from classical MD using an EAM potential) is too great to be done by *ab intio* MD using our available resources. Nevertheless, this preliminary study exposes promising features through our direct comparison of Al_3Ti (112) with TiB_2 (0001). We find some evidence that Al_3Ti (112) is a more powerful nucleant than TiB_2 (0001) with signs that continu-

ous growth of fcc structure on top of Al_3Ti (112) is possible. This can be seen as supporting the accepted view that "free growth" occurs on Al_3Ti (112) which coats TiB_2, as suggested by previous experiments.[40–43] However, these simulations suggest a second possibility, namely, that strained Al grows on the Ti-terminated surface of TiB_2, and it is this surface on which growth occurs.

To conclude, while these simulations have raised interesting possibilities, we recognize that they are just a first step. Longer and larger simulations are needed, as well as further experimentation, to fully understand the mechanisms of nucleation.

ACKNOWLEDGMENTS

The authors would like to acknowledge funding and computational resources provided by the King Abdullah University of Science and Technology.

[1] A. Cibula and R. W. Ruddle, J. Inst. Met. **76**, 361 (1949).
[2] A. L. Greer, Philos. Trans. R. Soc. London, Ser. B **361**, 479 (2003).
[3] B. Cantor and R. D. Doherty, Acta Metall. **27**, 33 (1979).
[4] K. A. Q. O'Reilly, B. Cantor, and P. G. Enright, Scr. Metall. Mater. **28**, 173 (1993).
[5] B. Cantor, Mater. Sci. Eng., A **226-228**, 151 (1997).
[6] B. Cantor, Philos. Trans. R. Soc. London, Ser. A **361**, 409 (2003).
[7] P. S. Mohanty and J. E. Gruzleski, Acta Mater. **44**, 3749 (1996).
[8] P. Schumacher and A. L. Greer, in *Light Metals*, edited by W. Hale (TMS, Anaheim, USA, 1996), p. 745.
[9] P. Schumacher and B. J. McKay, J. Non-Cryst. Solids **317**, 123 (2003).
[10] N. Iqbal, N. H. van Dijk, S. E. Offerman, M. P. Moret, L. Katgerman, and G. J. Kearley, Acta Mater. **53**, 2875 (2005).
[11] N. Iqbal, N. H. van Dijk, S. E. Offerman, N. Geerlofs, M. P. Moret, L. Katgerman, and G. J. Kearley, Mater. Sci. Eng., A **416**, 18 (2006).
[12] N. Iqbal, N. H. van Dijk, S. E. Offerman, M. P. Moret, L. Katgerman, and G. J. Kearley, J. Non-Cryst. Solids **353**, 3640 (2007).
[13] G. Kresse and J. Hafner, Phys. Rev. B **47**, 558 (1993).
[14] G. Kresse and J. Hafner, Phys. Rev. B **49**, 14251 (1994).
[15] G. Kresse and J. Furthmüller, Comput. Mater. Sci. **6**, 15 (1996).
[16] G. Kresse and J. Furthmüller, Phys. Rev. B **54**, 11169 (1996).
[17] P. E. Blöchl, Phys. Rev. B **50**, 17953 (1994).
[18] G. Kresse and J. Joubert, Phys. Rev. B **59**, 1758 (1999).
[19] J. P. Perdew, J. A. Chevary, S. H. Vosko, K. A. Jackson, M. R. Pederson, D. J. Singh, and C. Fiolhais, Phys. Rev. B **46**, 6671 (1992).
[20] J. P. Perdew, J. A. Chevary, S. H. Vosko, K. A. Jackson, M. R. Pederson, D. J. Singh, and C. Fiolhais, Phys. Rev. B **48**, 4978 (1993).
[21] E. R. Davidson, in *Methods in Computational Molecular Physics*, edited by G. H. F. Diercksen and S. Wilson, Vol. 113 of NATO Advanced Study Institute, Series C: (Plenum, New York, 1983), p. 95.
[22] D. M. Wood, J. Phys. A **18**, 1343 (1985).
[23] P. Norby and A. Norlund Christensen, Acta Chem. Scand., Ser. A **40a**, 157 (1986).
[24] R. G. Munro, J. Res. Natl. Inst. Stand. Technol. **105**, 709 (2000).
[25] R. R. Zope and Y. Mishin, Phys. Rev. B **68**, 024102 (2003).
[26] W. G. Hoover, Phys. Rev. A **31**, 1695 (1985).
[27] S. Plimpton, P. Crozier, and A. Thompson, LAMMPS, http://lammps.sandia.gov, Sandia National Laboratories, Albuquerque, NM, USA, 2009).
[28] D. Alfè, L. Vočadlo, G. Price, and M. Gillan, J. Phys.: Condens. Matter **16**, S973 (2004).
[29] A. Hashibon, J. Adler, M. W. Finnis, and W. D. Kaplan, Comput. Mater. Sci. **24**, 443 (2002).
[30] D. Buta, M. Asta, and J. J. Hoyt, Phys. Rev. E **78**, 031605 (2008).
[31] J. D. Honeycutt and H. C. Andersen, J. Phys. Chem. **91**, 4950 (1987).
[32] C. L. Kelchner, S. J. Plimpton, and J. C. Hamilton, Phys. Rev. B **58**, 11085 (1998).
[33] H. Tsuzuki, P. S. Branicio, and J. P. Rino, Comput. Phys. Commun. **177**, 518 (2007).
[34] J. Morris and X. Song, J. Chem. Phys. **119**, 3920 (2003).
[35] M. P. Allen and D. J. Tildesley, *Computer Simulation of Liquids* (Oxford University Press, Oxford, 1987).
[36] J. R. Morris, C. Z. Wang, K. M. Ho, and C. T. Chan, Phys. Rev. B **49**, 3109 (1994).
[37] *CRC Handbook of Chemistry and Physics*, edited by D. R. Lide (CRC Press, Boca Raton, 2009).
[38] I. Loa, K. Kunc, K. Syassen, and P. Bouvier, Phys. Rev. B **66**, 134101 (2002).
[39] A. Smakula and J. Kalnajs, Phys. Rev. **99**, 1737 (1955).
[40] I. Maxwell and A. Hellawell, Acta Metall. **23**, 229 (1975).
[41] A. L. Greer, A. M. Bunn, A. Tronche, P. V. Evans, and D. J. Bristow, Acta Mater. **48**, 2823 (2000).
[42] P. Schumacher, A. L. Greer, J. Worth, P. V. Evans, M. A. Kearns, P. Fisher, and A. H. Green, Mater. Sci. Technol. **14**, 394 (1998).
[43] M. Easton, Metall. Mater. Trans. A **36A**, 1911 (2005).